Supporting Information

Orbital Model Unraveling Slipped-Stacking Induced Quantum Interference in Tetrahedral 2D Conjugated Polymers

Yang Li,[a] Zhenling Liu,[bc] Shaoqing Guan,[bc] Dan Liu,[b] Qingbin Li,[b] Can Gao,[b] Yongshuai Wang,[b] Jichen Dong,[b] Wenping Hu,[d] Yunqi Liu,[b] and Huanli Dong*[bc]*

[a.] *College of Science, Shenyang University, Shenyang 110044, China.*

b. Beijing National Laboratory for Molecular Science, Key Laboratory of Organic Solids, Institute of Chemistry, Chinese Academy of Sciences, Beijing 100190, China.

[c.] *University of Chinese Academy of Science, Beijing 100049, China.*

[d.] *Tianjin Key Laboratory of Molecular Optoelectronic Sciences, Department of Chemistry, School of Science, Tianjin University and Collaborative Innovation Center of Chemical Science and Engineering, Tianjin 300072, China.*

*Correspondence to: dhl522@iccas.ac.cn and dongjichen@iccas.ac.cn

CONTENTS

1. Additional fitting parameters

Table S1 Tight-binding parameters for the single-orbital model (in meV).

	p-TBTBP		p-3-TBQP		p-2-TBQP		p-TBTTA	
	CB	VB	CB	VB	CB	VB	CB	VB
ε	1801	-311	1375	-97	1131	-240	1525	-255
t_1	9	-15	52	-42	-5	-13	73	-116
t_2	17	-136	-6	10	2	-96	-45	55
t_3	4	11	-6	25	1	2	-20	50

Table S2 Tight-binding parameters for the double-orbital model (in meV)

	separated double orb		crossed double orb			
	p-TBTBP	p-2-TBQP	p-3-TBQP		p-TBTTA	
	VB	VB	VB	CB	VB	CB
ε	-635	-741	-267	1936	-480	1848
t_0	-68	85	100	536	91	200
t_1	-287	-391	-102	108	-204	209
t_2	7	-136	-9	2	0	-39
t_3	\	46	0	-8	9	11

Table S3 Tight-binding parameters for the separated triple-orbital model and Lieb-like model (in meV)

	Lieb-like		separated triple orb
	p-TBTBP	p-2-TBQP	p-2-TBQP
	CB	VB	VB
ε	2717	-832	-777
$\Delta\varepsilon$	-897	322	156
t_0	81	116	170
t_1	49	28	-338
t_2	-276	-338	4
t_3	24	0	\
t_4	6	0	\

Table S4 Tight-binding parameters of the interlayer interactions (in meV)

	Single orb			separated double orb	crossed double orb		Lieb-like		separated triple orb
	p-TBTBP	p-3-TBQP	p-2-TBQP	p-TBTBP	p-3-TBQP	p-3-TBQP	p-TBTBP	p-2-TBQP	p-2-TBQP
	CB	CB	CB	VB	VB	CB	CB	VB	VB
ε'	1715	1299	1121	-734	-377	1866	2635	-858	-807
a_1	6	-14	15	97	-154	82	-4	-29	-29
a_2	\	\	\	97	148	-55	65	-50	-50
a_3	\	\	\	\	\	\	65	-50	-50
d_1	21	17	10	4	16	4	0	0	0
d_2	0	13	0	0	0	-35	-90	0	140
d_3	-21	-15	4	0	0	-29	0	153	-85
d_4	0	0	0	\	0	32	0	-90	\

d_5	\	\	\	\	0	0	90	\	\

Table S5 Tight-binding parameters of the interlayer interactions for p-3-TBQP under more interlayer slipping (in meV)

	crossed double orb	
	p-3-TBQP (lateral slipped)	p-3-TBQP (eclipsed)
	VB	CB
ε'	-460	-286
a_1	-48	199
a_2	-48	199
a_3	\	\
d_1	32	6
d_2	77	0
d_3	0	0
d_4	77	0
d_5	0	0

2. Recombined-orbital analysis on more 2DCPs

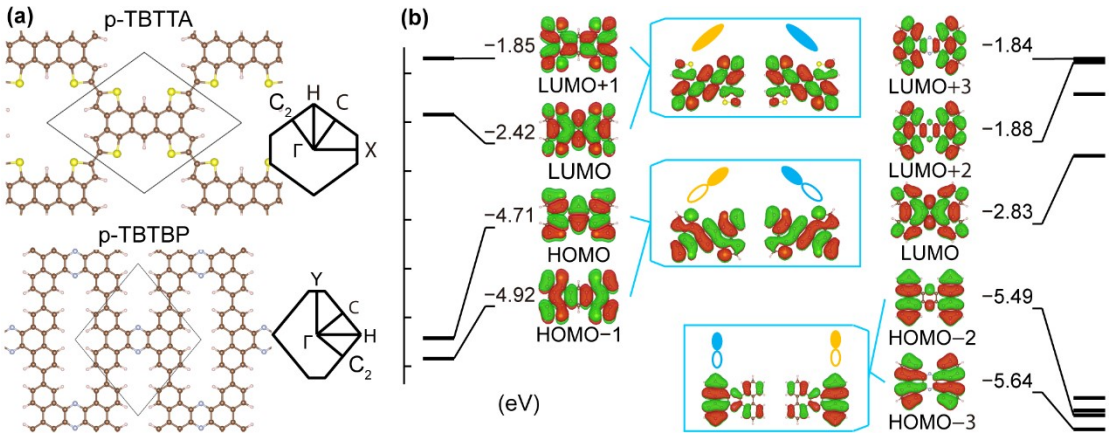

Fig. S1 (a) Geometric structures of p-TBTTA and p-TBTBP with their first Brillouin zones. (b) Wavefunctions of the original molecular orbitals of the hydrogen-passivated building blocks, along with some recombined molecular orbitals derived from them.

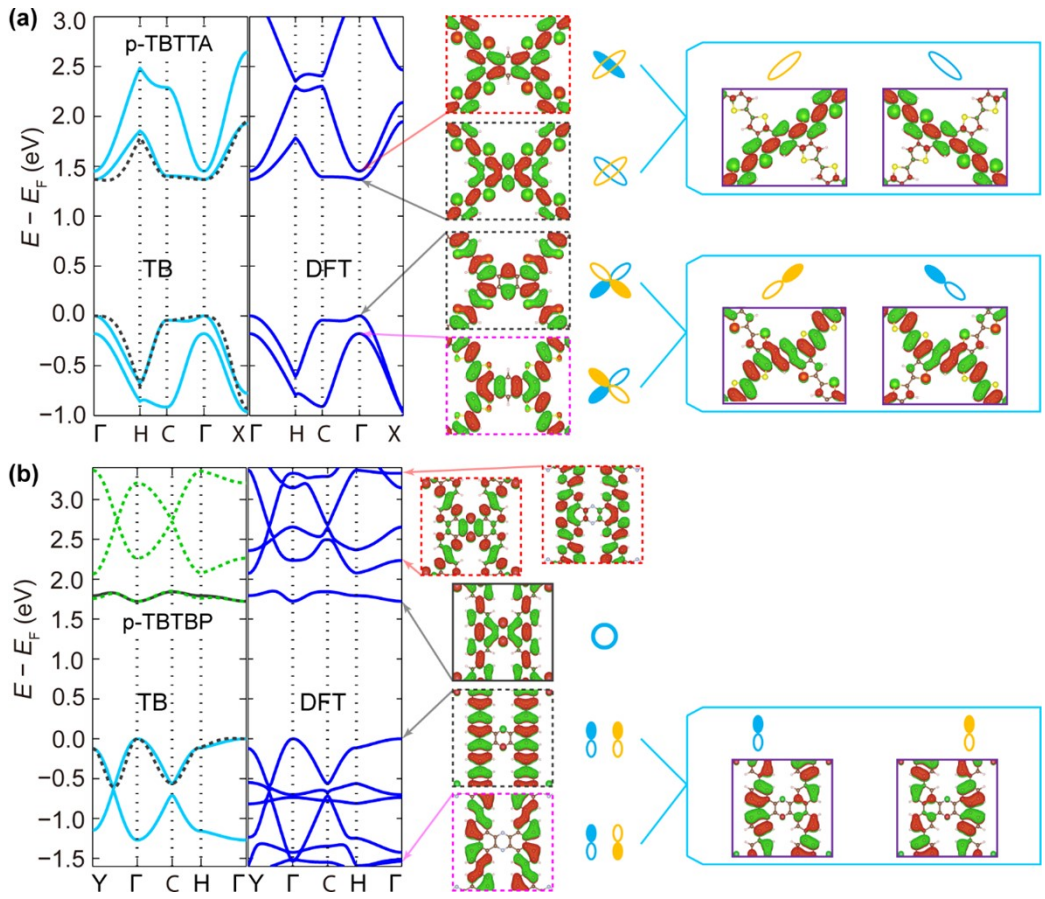

Fig. S2 Energy bands at the TB and DFT levels for (a) p-TBTTA, and (b) p-TBTBP. In the TB bands, grey, light blue, and light green lines are used to differentiate between single-orbital, double-orbital, and Lieb-like models respectively; solid lines indicate results obtained by the preferred model in contrast to others. Inset: pseudo wavefunctions at the Γ point corresponding to molecular orbitals depicted in Figure S1b, along with the recombined orbital basis derived from them.

3. Additional information regarding the recombined-orbital model

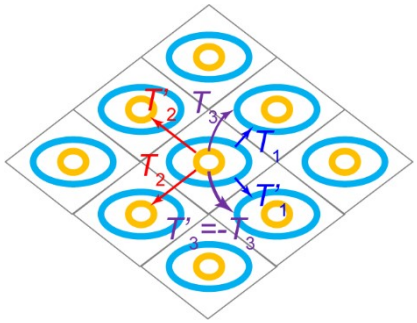

Fig. S3 Illustration of the orbital based tight-binding model using double-orbital basis, *i.e.*, orbital 1 (blue) with an on-site energy ε and orbital 2 (orange) with an on-site energy $\varepsilon + \Delta\varepsilon$. According to symmetry of common tetrahedral 2DCPs compatible to the crossed double-orbital model, $T_1 = T_1'$, $T_2 = T_2'$, while $T_3 = -T_3'$.

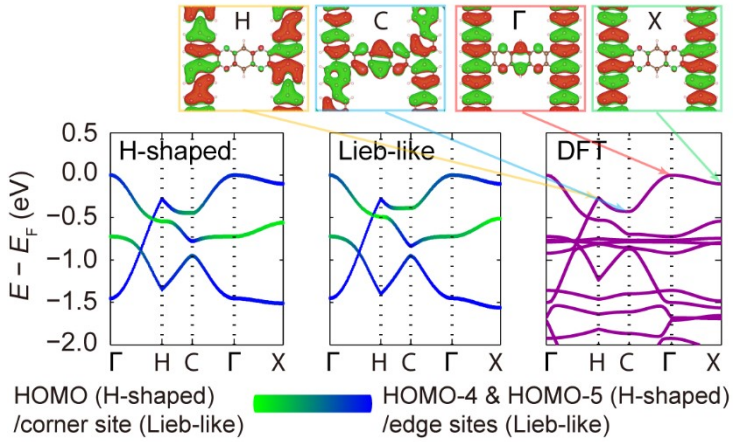

Fig. S4 Projected energy bands analysis of the VB of p-2-TBQP, combined with the wavefunctions at different reciprocal space high-symmetry points.

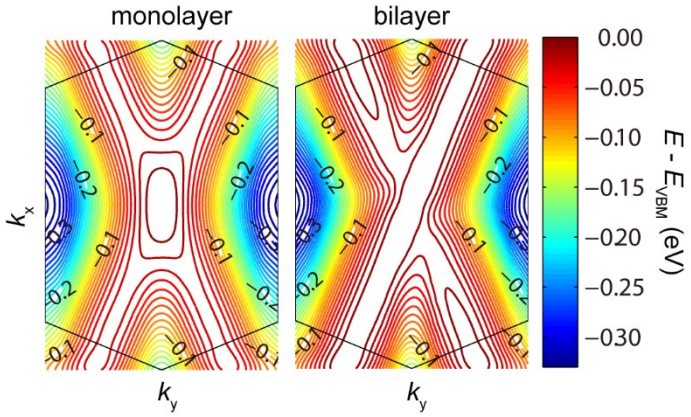

Fig. S5 Comparison of the contour maps of the energy band of monolayer and bilayer p-3-TBQP. The first Brillioun region is illustrated by black solid lines.

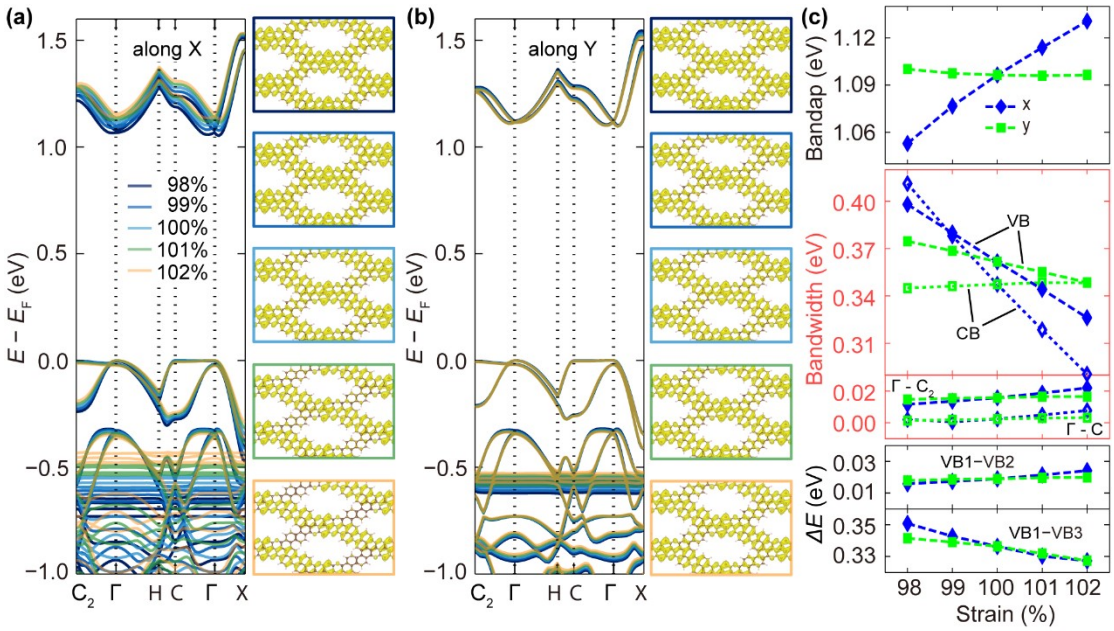

Fig. S6 Influence of uniaxial strain on the p-3-TBQP bilayer. (a-b) Evolution of band structures, as well as charge distributions within an energy range of ($-\frac{1}{2}kT,\frac{1}{2}kT$) centered at the VB maximum, with uniaxial strain varying from 98% to 102% along (a) the x-axis, corresponding to the armchair direction, and (b) the y-axis, corresponding to the zigzag direction. (c) Strain dependence of bandgaps, bandwidths, and energy differences at Γ, using identical y-axis scaling for direct comparison of energies across subpanels. The dashed lines are drawn as visual guides.

From Figure S6c, it can be seen that interlayer interaction, quantified by the energy difference between the highest and third-highest VB at Γ, decreases slowly as strain increases in either direction. In contrast, intralayer interaction, as measured by the bandwidth of the highest VB, exhibits a rapid decline when subjected to strain along armchair direction but responds slowly under stress applied along zigzag direction. Therefore, fluctuations in interference can be attributed to subtle changes in intralayer interactions driven by in-plane charge redistribution.

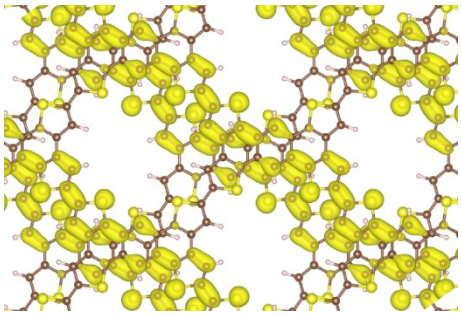

Fig. S7 Charge distribution within an energy range of ($-kT,kT$) centered at the CB minimum in the p-TBTTA bilayer (at a local minima of interlayer slipping, as detailed in Reference 51 of the main text).

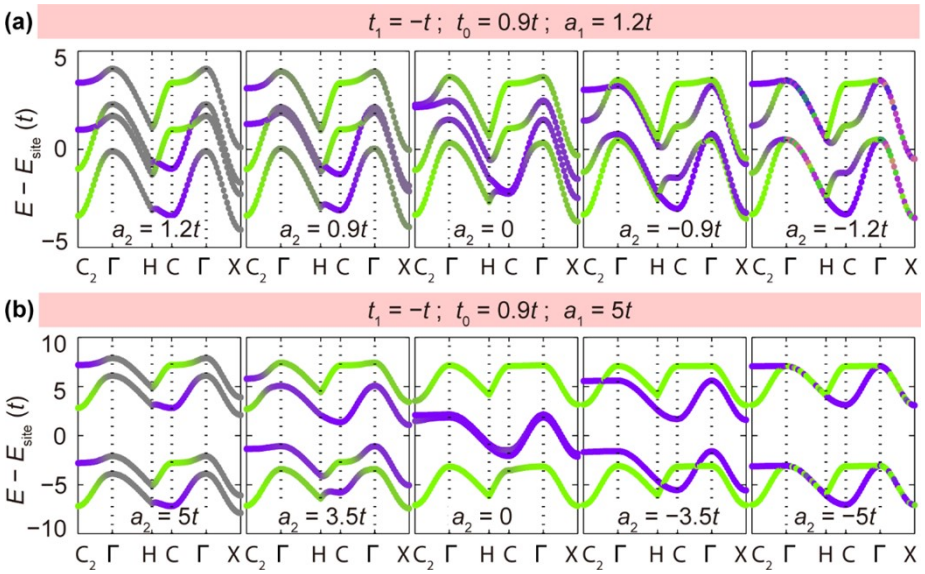

Fig. S8 Projected energy bands analysis of model tetrahedral systems with double layers. The angle between R_1 and R_2 is fixed at 60°.

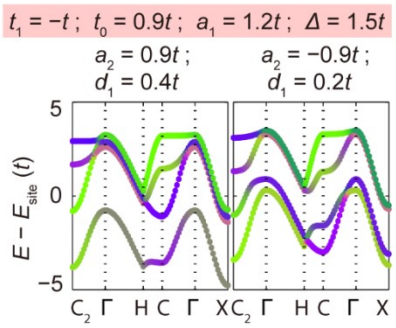

Fig. S9 Projected energy bands analysis of model tetrahedral systems with double layers with a vertical electric field. The angle between R_1 and R_2 is fixed at 60°.

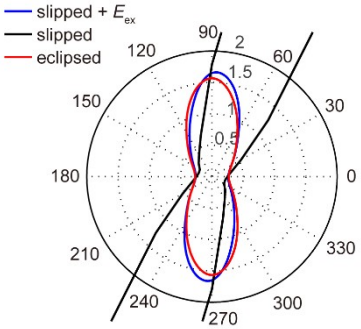

Fig. S10 Hole effective masses in the unit electron effective mass (m_e) of bilayer p-3-TBQP with different interlayer offset. E_{ex} is 0.2 eV Å^{-1}.

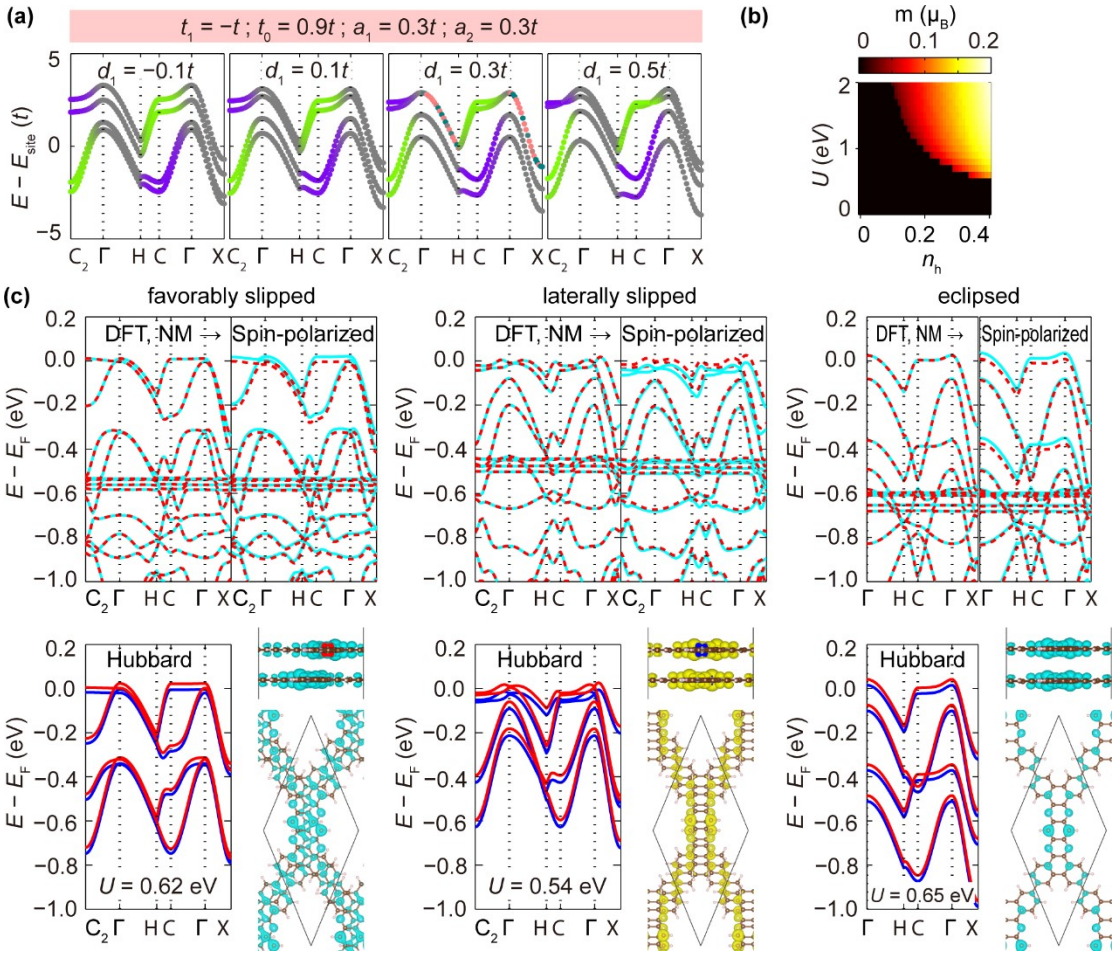

Fig. S11 (a) Projected energy bands of a model tetrahedral system with bands facilitating the Stoner magnetism hybridized near the Fermi level. (b) Magnetic moment of p-3-TBQP per layer in an interlayer antiparallel magnetic order with respect to hole doping concentration n_h and Coulomb repulsion U. (c) Spin-polarized energy bands calculated by DFT and the model Hamiltonian. Inset: Spin density drawn with an isosurface of 2×10^{-4}.

4. Band structures obtained at higher levels of theory

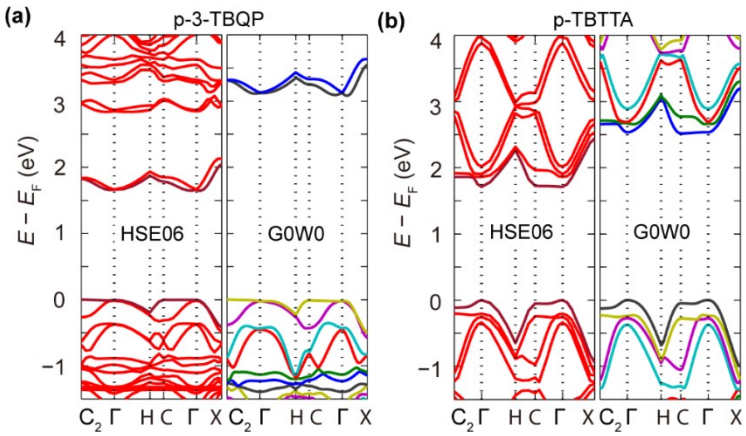

Fig. S12 Energy bands obtained by the screened hybrid functinal HSE06 and single-shot G_0W_0 constructed over PBE orbitals using Wannier interpolation for (a) p-3-TBQP bilayer, and (b) p-TBTTA bilayer, the latter adopting a interlayer slipping at a local minima.

Table S6 Bandwidths along Γ-C_1 and Γ-C_2, and energy differences between the bands nearest and next nearest to the Fermi level at Γ under different levels of theory. (in meV)

	p-3-TBQP (VB)			p-TBTTA (CB)			p-TBTTA (VB)		
	Γ-C_1	Γ-C_2	ΔE (Γ)	Γ-C_1	Γ-C_2	ΔE (Γ)	Γ-C_1	Γ-C_2	ΔE (Γ)
PBE	2	16	19	6	126	128	54	105	180
HSE06	1	11	13	12	149	149	55	114	206
G_0W_0	10	22	0	18	127	137	55	126	236

To evaluate the limitations of pure functionals in accurately describing bandgaps and charge transfer properties, we also conducted calculations employing the screened hybrid functional HSE06 and the many-body GW approximation. Specifically, quasiparticle bands were obtained through single-shot GW calculations (G_0W_0) constructed over PBE orbitals, with subsequent Wannier interpolations. Due to server memory constraints, the reciprocal space grid mesh for these calculations was set to 3×3×1. Furthermore, in the G_0W_0 calculations, we reduced computational precision by setting a vacuum height exceeding 10 Å and an energy cutoff of 300 eV.

The p-3-TBQP bilayer (fully relaxed) and the p-TBTTA bilayer (at a local minimum of interlayer slipping, as detailed in Reference 51 of the main text) were chosen due to their typical band dispersion characteristics. The VB of the former and both the VB and the CB of the latter are compatible with the crossed double-orbital model that is our primary focus. Results presented in Figure S10 indicate no significant changes in the band structures compared to those obtained using PBE. Specifically, the narrowness along the Γ-C_1 and Γ-C_2 directions, dispersion in the Γ-X direction, and energy splitting arising from interlayer interactions are well preserved for π-bands near the Fermi level. Table S5 summarizes the anisotropy in electronic structures as measured by bandwidth along Γ-C_1 and Γ-C_2. According to these results, electronic anisotropy remains robust, while bandwidth magnitute is method-dependent. In p-3-TBQP, both at PBE and HSE06 levels, VB bandwidth along Γ-C_1 is an order of magnitude smaller

than that along Γ-C_2; conversely, G_0W_0 calculations show that it is half as large as that along Γ-C_2. This may render charge density transitions driven by electronic interference less pronounced at the G_0W_0 level. Beyond the influence of low computational precision in G_0W_0 calculations, the sensitivity in bandwidth can be attributed to the small absolute values. In contrast, for the p-TBTTA bilayer, the relative bandwidths along Γ-C_1 and Γ-C_2 remain consistent for both VB and CB owing to their larger absolute values. Consequently, while there may be minor differences in the fitting parameters, their influence on the overall charge distribution becomes negligible, and the quasi-one-dimensional charge redistribution around CB minimum resulting from interlayer interference (see Figure S7) remains unaffected with respect to theoretical methods. In conclusion, varying theoretical methods exert little substantial impact on our discussions on interlayer interactions and quantum interference. Therefore, considering the computational resource constraints, results based on the PBE functional are used in the main text.

5. Geometries of the DFT optimized structures

Table S7 Lattice vectors and fractional atomic coordinates of monolayer and bilayer p-3-TBQP (in Å)

a	15.779500	-6.512899	0.000000	***a***	15.769879	-6.513591	0.000000
b	15.779500	6.512899	0.000000	***b***	15.769879	6.513591	0.000000
c	0.000000	0.000000	16.000000	***c***	0.000000	0.000000	19.500000
Element	***a***	***b***	***c***	Element	***a***	***b***	***c***
C	0.365852	0.252786	0.485044	C	0.366066	0.252550	0.400932
C	0.459062	0.237575	0.486460	C	0.459169	0.237513	0.401534
C	0.566499	0.128879	0.487521	C	0.566607	0.128904	0.401887
C	0.582786	0.037211	0.487666	C	0.583021	0.037144	0.401612
C	0.491913	0.049106	0.486251	C	0.492209	0.048905	0.400779
C	0.385375	0.157751	0.484592	C	0.385639	0.157468	0.400374
C	0.252716	0.365945	0.485053	C	0.252991	0.365590	0.401409
C	0.237554	0.459124	0.486506	C	0.237860	0.458776	0.402207
C	0.157653	0.385523	0.484584	C	0.157913	0.385139	0.401447
C	0.049024	0.492078	0.486245	C	0.049304	0.491799	0.402004
C	0.037170	0.582925	0.487694	C	0.037576	0.582577	0.402630
C	0.128874	0.566586	0.487579	C	0.129277	0.566224	0.402728
C	0.444302	0.332881	0.487372	C	0.444512	0.332707	0.402463
C	0.332894	0.444305	0.487423	C	0.333153	0.444021	0.402952
C	0.517410	0.405832	0.489484	C	0.517595	0.405725	0.403942
C	0.405904	0.517347	0.489578	C	0.406103	0.517205	0.404625
C	0.609432	0.390864	0.490267	C	0.609538	0.390876	0.404073
C	0.594471	0.482884	0.490712	C	0.594604	0.482888	0.404405
C	0.482958	0.594393	0.490811	C	0.483118	0.594376	0.404881
C	0.390942	0.609358	0.490468	C	0.391106	0.609279	0.405462
C	0.667431	0.555996	0.490176	C	0.667613	0.555966	0.404047
C	0.556006	0.667411	0.490246	C	0.556288	0.667310	0.403965
C	0.762740	0.541232	0.489283	C	0.762866	0.541295	0.403578
C	0.747522	0.634452	0.488363	C	0.747816	0.634423	0.402048
C	0.842544	0.614934	0.487254	C	0.842847	0.614894	0.401261
C	0.951203	0.508375	0.487027	C	0.951372	0.508315	0.402247
C	0.963113	0.417485	0.487885	C	0.963141	0.417519	0.403933

C	0.871442	0.433780	0.488973	C	0.871416	0.433872	0.404495
C	0.634365	0.747588	0.488382	C	0.634773	0.747477	0.401714
C	0.541180	0.762757	0.489370	C	0.541558	0.762622	0.403019
C	0.433709	0.871440	0.489122	C	0.434122	0.871197	0.403519
C	0.417351	0.963148	0.488024	C	0.417849	0.962843	0.402665
C	0.508209	0.951285	0.487068	C	0.508657	0.951053	0.401078
C	0.614789	0.842642	0.487232	C	0.615246	0.842500	0.400661
H	0.636929	0.119091	0.488607	C	0.319459	0.375432	0.577810
H	0.314073	0.169266	0.483163	C	0.412662	0.360319	0.578268
H	0.169131	0.314247	0.483134	C	0.520116	0.251757	0.578859
H	0.119130	0.636992	0.488691	C	0.536402	0.160097	0.579223
H	0.831006	0.686258	0.486448	C	0.445594	0.171865	0.578587
H	0.881244	0.363332	0.489631	C	0.339007	0.280389	0.577641
H	0.363298	0.881189	0.489837	C	0.206408	0.488479	0.577502
H	0.686089	0.831139	0.486326	C	0.191348	0.581630	0.577533
H	0.693179	0.307112	0.490139	C	0.111392	0.507974	0.577304
H	0.307194	0.693106	0.490490	C	0.002863	0.614568	0.577320
H	0.667758	0.955077	0.489205	C	0.991075	0.705398	0.577513
H	0.955047	0.667913	0.489227	C	0.082793	0.689063	0.577502
H	0.045266	0.332485	0.487834	C	0.397915	0.455645	0.578012
H	0.332336	0.045284	0.488039	C	0.286585	0.566984	0.577801
N	0.533386	0.315494	0.488445	C	0.471074	0.528587	0.577895
N	0.315544	0.533364	0.488588	C	0.359582	0.640077	0.578230
N	0.684815	0.466907	0.490609	C	0.563086	0.513677	0.577332
N	0.466945	0.684757	0.490775	C	0.548090	0.605750	0.577707
				C	0.436598	0.717237	0.578321
				C	0.344652	0.732090	0.578478
				C	0.621048	0.678932	0.577882
				C	0.509701	0.790245	0.578506
				C	0.716340	0.664177	0.577681
				C	0.701228	0.757347	0.577040
				C	0.796320	0.737762	0.576322
				C	0.904920	0.631096	0.577111
				C	0.916629	0.540333	0.577914
				C	0.824910	0.556719	0.577984
				C	0.588160	0.870390	0.577633
				C	0.495063	0.885428	0.578757
				C	0.387644	0.994030	0.579700
				C	0.371243	0.085780	0.579823
				C	0.462051	0.074018	0.578617
				C	0.568594	0.965467	0.577329
				H	0.636905	0.119366	0.402616
				H	0.314384	0.168834	0.399850
				H	0.169384	0.313810	0.400576

				H	0.119658	0.636555	0.403874
				H	0.831408	0.686169	0.400238
				H	0.880947	0.363586	0.405634
				H	0.363796	0.880848	0.405310
				H	0.686618	0.830943	0.399873
				H	0.693275	0.307169	0.403780
				H	0.307375	0.692959	0.406416
				H	0.668017	0.954997	0.402272
				H	0.955490	0.667547	0.403743
				H	0.045256	0.332504	0.404791
				H	0.332916	0.044944	0.403805
				H	0.590446	0.242157	0.578661
				H	0.267674	0.291904	0.576326
				H	0.122859	0.436673	0.576672
				H	0.073235	0.759368	0.577738
				H	0.784852	0.809095	0.575729
				H	0.834513	0.486387	0.578035
				H	0.317349	0.003556	0.580459
				H	0.639809	0.954128	0.575804
				H	0.646812	0.429992	0.576429
				H	0.260916	0.815801	0.578642
				H	0.621367	0.077998	0.579817
				H	0.908953	0.790418	0.577989
				H	0.998713	0.455334	0.578215
				H	0.286255	0.167921	0.581033
				N	0.533613	0.315341	0.403039
				N	0.315716	0.533171	0.404309
				N	0.684992	0.466870	0.404176
				N	0.467118	0.684750	0.404651
				N	0.487082	0.438213	0.577942
				N	0.269199	0.656085	0.578149
				N	0.638479	0.589774	0.577373
				N	0.420592	0.807620	0.578696

Table S8 Lattice vectors and fractional atomic coordinates of monolayer and bilayer p-2-TBQP (in Å)

a	11.968463	-8.685420	0.000000	***a***	11.971745	-8.680749	0.000000
b	11.968463	8.685420	0.000000	***b***	11.971745	8.680749	0.000000
c	0.000000	0.000000	16.000000	***c***	0.000000	0.000000	19.500000
Element	***a***	***b***	***c***	Element	***a***	***b***	***c***
C	0.290712	0.206726	0.488866	C	0.291318	0.206812	0.402729
C	0.383290	0.216223	0.490981	C	0.383845	0.216223	0.404857
C	0.463795	0.135059	0.492054	C	0.464311	0.134991	0.406124
C	0.457215	0.042678	0.490829	C	0.457745	0.042630	0.404923
C	0.364546	0.034300	0.488139	C	0.365088	0.034341	0.402650

C	0.284447	0.113516	0.487292	C	0.285020	0.113655	0.401626
C	0.206645	0.290875	0.488830	C	0.207257	0.290939	0.402562
C	0.216282	0.383382	0.490994	C	0.216729	0.383454	0.404824
C	0.113399	0.284742	0.487113	C	0.114057	0.284771	0.400617
C	0.034294	0.364933	0.487944	C	0.034873	0.364959	0.401069
C	0.042783	0.457547	0.490766	C	0.043235	0.457566	0.403930
C	0.135207	0.463992	0.492056	C	0.135583	0.464071	0.405693
C	0.394899	0.311069	0.492132	C	0.395364	0.311037	0.406168
C	0.311211	0.394808	0.492182	C	0.311632	0.394761	0.406413
C	0.491273	0.407455	0.493870	C	0.491655	0.407394	0.408114
C	0.407727	0.491024	0.493975	C	0.408087	0.490979	0.408534
C	0.582197	0.418160	0.494451	C	0.582519	0.418105	0.408462
C	0.592926	0.509076	0.494911	C	0.593211	0.508987	0.408836
C	0.509357	0.592619	0.495036	C	0.509628	0.592560	0.409078
C	0.418454	0.581915	0.494688	C	0.418727	0.581903	0.409337
C	0.689312	0.605473	0.494848	C	0.689622	0.605251	0.408506
C	0.605561	0.689160	0.494940	C	0.605862	0.689002	0.408408
C	0.784179	0.617070	0.494239	C	0.784450	0.616815	0.407570
C	0.793682	0.709661	0.493882	C	0.793888	0.709392	0.406388
C	0.886881	0.715963	0.493037	C	0.887002	0.715759	0.405050
C	0.966074	0.635849	0.492114	C	0.966256	0.635720	0.404326
C	0.957703	0.543139	0.492190	C	0.958022	0.543021	0.405185
C	0.865335	0.536548	0.493536	C	0.865718	0.536325	0.407248
C	0.709525	0.793723	0.493852	C	0.709767	0.793473	0.406443
C	0.616979	0.784088	0.494324	C	0.617211	0.783934	0.407434
C	0.536343	0.865165	0.493669	C	0.536618	0.865102	0.407340
C	0.542823	0.957579	0.492196	C	0.543226	0.957440	0.405755
C	0.635485	0.966083	0.491884	C	0.635875	0.965840	0.404854
C	0.715672	0.886982	0.492806	C	0.715975	0.886656	0.405418
H	0.532317	0.148112	0.494076	C	0.278461	0.320108	0.580386
H	0.354637	0.964285	0.486645	C	0.370995	0.329679	0.581819
H	0.215009	0.102347	0.485401	C	0.451593	0.248533	0.582330
H	0.102065	0.215396	0.485108	C	0.445011	0.156180	0.581214
H	0.964232	0.355151	0.486328	C	0.352408	0.147742	0.579293
H	0.148419	0.532430	0.494109	C	0.272299	0.226911	0.578880
H	0.898100	0.785393	0.492841	C	0.194332	0.404172	0.580342
H	0.036090	0.645774	0.491074	C	0.203785	0.496746	0.581240
H	0.852240	0.468026	0.494019	C	0.101206	0.397816	0.579319
H	0.467825	0.852031	0.494282	C	0.021943	0.477856	0.579622
H	0.645312	0.036133	0.490643	C	0.030184	0.570549	0.581090
H	0.785073	0.898289	0.492411	C	0.122525	0.577226	0.581611
H	0.644978	0.355336	0.494301	C	0.382352	0.424615	0.582176
H	0.355683	0.644741	0.494716	C	0.298593	0.508358	0.581823
N	0.481965	0.318586	0.493018	C	0.478572	0.521066	0.582499

N	0.318826	0.481818	0.493171	C	0.394981	0.604643	0.582555
N	0.681793	0.518405	0.494929	C	0.569468	0.531723	0.582209
N	0.518549	0.681525	0.495147	C	0.580107	0.622652	0.582537
				C	0.496540	0.706245	0.582889
				C	0.405671	0.695532	0.582828
				C	0.676580	0.718883	0.582772
				C	0.592855	0.802615	0.583116
				C	0.771496	0.730197	0.582644
				C	0.781007	0.822739	0.582525
				C	0.874231	0.828920	0.582152
				C	0.953383	0.748718	0.581829
				C	0.944991	0.656042	0.581826
				C	0.852618	0.649537	0.582287
				C	0.696957	0.906865	0.582477
				C	0.604397	0.897438	0.582931
				C	0.523898	0.978662	0.582578
				C	0.530499	0.071004	0.581556
				C	0.623190	0.079308	0.580644
				C	0.703273	0.000015	0.581285
				H	0.532823	0.147940	0.408494
				H	0.355261	0.964302	0.401360
				H	0.215573	0.102561	0.399877
				H	0.102910	0.215369	0.398290
				H	0.964818	0.355230	0.399002
				H	0.148602	0.532520	0.408425
				H	0.898037	0.785233	0.404776
				H	0.036270	0.645593	0.403187
				H	0.852786	0.467744	0.408420
				H	0.468112	0.852070	0.408995
				H	0.645689	0.035864	0.404043
				H	0.785435	0.897762	0.405268
				H	0.645340	0.355278	0.408182
				H	0.355897	0.644700	0.409929
				H	0.520094	0.261621	0.583214
				H	0.342668	0.077730	0.577250
				H	0.202893	0.215807	0.576714
				H	0.090178	0.328367	0.577663
				H	0.951935	0.467994	0.578207
				H	0.135529	0.645772	0.582644
				H	0.885433	0.898360	0.582364
				H	0.023457	0.758507	0.581504
				H	0.839526	0.581034	0.582059
				H	0.455328	0.965697	0.582930
				H	0.633026	0.149343	0.579385

				H	0.772754	0.011106	0.580648
				H	0.632295	0.468927	0.581553
				H	0.342847	0.758357	0.582885
				N	0.482411	0.318534	0.407119
				N	0.319181	0.481800	0.407893
				N	0.682102	0.518213	0.408706
				N	0.518813	0.681446	0.408907
				N	0.469395	0.432176	0.582433
				N	0.306093	0.595406	0.582192
				N	0.669011	0.631830	0.582364
				N	0.505802	0.795110	0.583156

Table S9 Lattice vectors and fractional atomic coordinates of monolayer and bilayer p-TBTBP (in Å)

a	7.188331	-8.684770	0.000000	***a***	7.181146	-8.676189	0.000000
b	7.188331	8.684770	0.000000	***b***	7.181146	8.676189	0.000000
c	0.000000	0.000000	16.000000	***c***	0.000000	0.000000	19.500000
Element	***a***	***b***	***c***	Element	***a***	***b***	***c***
C	0.456842	0.042222	0.492727	C	0.454397	0.039306	0.413113
C	0.495799	0.167437	0.492639	C	0.492953	0.164437	0.408613
C	0.415156	0.248579	0.492676	C	0.412289	0.245524	0.410662
C	0.288549	0.204639	0.492742	C	0.285941	0.201583	0.416219
C	0.249690	0.078126	0.492789	C	0.247614	0.075291	0.421733
C	0.330438	0.999725	0.492788	C	0.328650	0.996909	0.420854
C	0.460794	0.378600	0.492692	C	0.457792	0.375554	0.408444
C	0.204639	0.288549	0.492760	C	0.201918	0.285498	0.416440
C	0.248579	0.415156	0.492826	C	0.245599	0.412024	0.411403
C	0.378600	0.460794	0.492810	C	0.375577	0.457794	0.408720
C	0.167437	0.495799	0.492863	C	0.164318	0.492564	0.409998
C	0.042222	0.456842	0.492775	C	0.039158	0.453672	0.413948
C	0.999725	0.330438	0.492714	C	0.996926	0.327642	0.420154
C	0.078126	0.249690	0.492713	C	0.075516	0.246793	0.421244
C	0.543158	0.957778	0.492775	C	0.540592	0.954978	0.410377
C	0.504201	0.832563	0.492863	C	0.501310	0.829786	0.408351
C	0.584844	0.751421	0.492826	C	0.581926	0.748566	0.407588
C	0.711451	0.795361	0.492760	C	0.708705	0.792512	0.408197
C	0.750310	0.921874	0.492713	C	0.747814	0.919116	0.409085
C	0.669562	0.000275	0.492714	C	0.667040	0.997595	0.410408
C	0.539206	0.621400	0.492810	C	0.536131	0.618493	0.407287
C	0.795361	0.711451	0.492742	C	0.792498	0.708450	0.409173
C	0.751421	0.584844	0.492676	C	0.748356	0.581738	0.409267
C	0.621400	0.539206	0.492692	C	0.618315	0.536204	0.407744
C	0.832563	0.504201	0.492639	C	0.829339	0.500799	0.410966
C	0.957778	0.543158	0.492727	C	0.954679	0.539883	0.412437
C	0.000275	0.669562	0.492788	C	0.997380	0.666374	0.412576

C	0.921874	0.750310	0.492789	C	0.919065	0.747279	0.410987
H	0.207670	0.591432	0.492945	C	0.547409	0.329124	0.579827
H	0.591432	0.207670	0.492557	C	0.586682	0.454313	0.581857
H	0.153459	0.039837	0.492847	C	0.506053	0.535528	0.582620
H	0.294363	0.903026	0.492843	C	0.379269	0.491583	0.582004
H	0.903026	0.294363	0.492659	C	0.340158	0.364983	0.581111
H	0.039837	0.153459	0.492655	C	0.420953	0.286521	0.579789
H	0.792330	0.408568	0.492557	C	0.551838	0.665600	0.582918
H	0.408568	0.792330	0.492945	C	0.295463	0.575634	0.581027
H	0.846541	0.960163	0.492655	C	0.339605	0.702343	0.580937
H	0.705637	0.096974	0.492659	C	0.469651	0.747891	0.582461
H	0.096974	0.705637	0.492843	C	0.258619	0.783272	0.579238
H	0.960163	0.846541	0.492847	C	0.133273	0.744182	0.577764
N	0.419573	0.580427	0.492870	C	0.090568	0.617692	0.577633
N	0.580427	0.419573	0.492632	C	0.168891	0.536790	0.579217
				C	0.633601	0.244784	0.577092
				C	0.595028	0.119655	0.581594
				C	0.675691	0.038554	0.579542
				C	0.802027	0.082494	0.573984
				C	0.840377	0.208797	0.568474
				C	0.759359	0.287186	0.569355
				C	0.630188	0.908527	0.581759
				C	0.886047	0.998582	0.573764
				C	0.842378	0.872054	0.578797
				C	0.712409	0.826277	0.581478
				C	0.923652	0.791517	0.580198
				C	0.048801	0.830400	0.576245
				C	0.091025	0.956425	0.570037
				C	0.012443	0.037279	0.568956
				H	0.204347	0.588018	0.405742
				H	0.588237	0.204510	0.403453
				H	0.151850	0.037173	0.427462
				H	0.293448	0.900504	0.426663
				H	0.900431	0.291929	0.424694
				H	0.037460	0.150792	0.426012
				H	0.789014	0.405068	0.410537
				H	0.405542	0.789725	0.407746
				H	0.844123	0.957250	0.409929
				H	0.703056	0.094289	0.412802
				H	0.094081	0.702274	0.414923
				H	0.957454	0.843538	0.411910
				H	0.298942	0.878996	0.579664
				H	0.682447	0.494369	0.582459
				H	0.243847	0.326819	0.580264

	H	0.384958	0.189825	0.577384
	H	0.993866	0.581769	0.575292
	H	0.130527	0.440522	0.578305
	H	0.883613	0.696052	0.584452
	H	0.499742	0.079575	0.586771
	H	0.936136	0.246900	0.562746
	H	0.794537	0.383596	0.563549
	H	0.187506	0.992117	0.565492
	H	0.050536	0.133282	0.564185
	N	0.416343	0.577547	0.407540
	N	0.577467	0.416466	0.407669
	N	0.510509	0.867628	0.582526
	N	0.671638	0.706522	0.582648